THE ASTRONOMICAL JOURNAL VOLUME 109, NUMBER 4 APRIL 1995

THE SOLAR SYSTEM BEYOND NEPTUNE

DAVID C. JEWITT
Institute for Astronomy, University of Hawaii, 2680 Woodlawn Drive, Honolulu, Hawaii 96822
Electronic mail: jewitt@galileo.ifa.hawaii.edu

JANE X. LUU
Harvard University, Astronomy Department, 60 Garden Street, Cambridge, Massachusetts 02138
Electronic mail: luu@cfa.harvard.edu

Received 1994 September 12; revised 1994 November 30

ABSTRACT

We present the results of a deep optical survey for distant solar system objects. An area of 1.2 sq deg of the ecliptic has been imaged to apparent red magnitude 25, resulting in the detection of seven trans-Neptunian objects. These are the first detected members of a trans-Neptunian disk that comprises about 35 000 objects larger than 100 km in the 30–50 AU heliocentric distance range. We interpret the new measurements using a set of Monte Carlo models in which the effects of observational bias in the data are taken into account.

1. INTRODUCTION

Since 1987, we have conducted a systematic observational campaign to assess the contents of the outer solar system (Luu & Jewitt 1988, hereafter referred to as Paper I). Our program was initially motivated by the desire to understand the apparent emptiness of the outer solar system. The general absence of bodies amongst and beyond the gas-giant planets, as perceived in 1987, could be interpreted either as an effect of observational selection (distant objects are faint) or as an indication of a real depletion of such bodies, perhaps as a result of dynamical instabilities driven by perturbations from the gas-giant planets (Gladman & Duncan 1990). More recently, the old idea that the trans-Neptunian region might preserve remnants from the pre-planetary disk (Edgeworth 1949; Kuiper 1951; Whipple 1964; Fernandez 1980) has been revived (Duncan *et al.* 1988). Our first observational work on this problem exploited both charge-coupled device (CCD) imagers to study a small area of sky to faint limiting magnitudes, and photographic plates to study larger areas albeit to less faint limiting magnitudes. Our initial results were negative.

Following Paper I, we continued the search using a variety of CCDs on different telescopes both at Kitt Peak, Arizona and on Mauna Kea, Hawaii. Meanwhile, independent searches were reported by Kowal (1989; a photographic survey of 6400 sq deg to R magnitude $m_R \sim 19.5$), Levison & Duncan (1990; a CCD survey of 4.9 sq deg to V magnitude $m_V = 22.5$), Cochran *et al.* (1991), and Tyson *et al.* (1992). Like Paper 1, these searches revealed no objects beyond the orbit of Neptune.

In this paper, we present a survey of 1.2 sq deg of the sky made using a large-format (2048×2048 pixel) CCD on Mauna Kea. The first trans-Neptunian (1992 QB_1 at $R = 41$ AU) was discovered in the early phases of this survey (Jewitt & Luu 1993a) and a set of similar bodies has been more recently revealed. The uniform observational conditions and procedures used in the Mauna Kea survey provide an internally consistent data set with which to study the size and distance distributions of the trans-Neptunian objects. Additional objects detected in parallel but less deep surveys are also discussed at the end of this paper.

2. OBSERVATIONS

The present observations were taken at the $f/10$ Cassegrain focus of the University of Hawaii 2.2 m telescope, located on Mauna Kea. The detector was an antireflection coated Tektronix 2048×2048 pixel CCD, with an average quantum efficiency of 90% in the 6000 to 7000 Å region. No reimaging optics were used, so the only light losses (over and above those at the primary and secondary mirror reflections) were due to reflection from the CCD dewar window and filter (about 4% each). The image scale was 0.219 arcsec per 24 μm pixel, giving a field of view 448 arcsec (0.12 deg) on a side. All images were taken through a Mould R filter centered at 6500 Å and with 1200 Å full width at half maximum (FWHM). This filter is optimum, since it includes the peak in the quantum efficiency of the CCD, yet excludes bright night sky emission lines due to atmospheric OH at longer wavelengths. An integration time of 900 s was selected so that the apparent motion of a trans-Neptunian object would not exceed the FWHM of the seeing disk on the best nights (0.6 to 0.7 arcsec). Therefore, "trailing loss" caused by spreading the light over many pixels, is negligible in the present data.

The observational procedure was similar to that described in Paper I. Observing at opposition allows us to estimate the distance to an object directly from its motion. We imaged ecliptic fields within 1.5 hr of opposition. Observations were confined to moonless skies. Interference from stars in the galactic plane was minimized by observing near the Spring and Autumnal equinoxes, when the galactic latitude of the opposition point is large. Each field was imaged four times to provide a sequence of images for blinking. The first three images were consecutive (image centers are about 1050 s apart) while the fourth was separated from the first by two or more hours. Typically, the first three images are used to identify moving objects while the fourth provides immediate

 0004-6256/95/109(4)/1867/10/$0.90

confirmation. The four images of each field were dithered by ~20 arcsec in order to allow the construction of a night sky median flat using the combined survey data from each night. A list of the field centers and dates of observation is given in Table 1. A sample image is shown in Fig. 1 (Plate 66).

Four observational criteria were employed to locate candidate distant solar system objects in the CCD images. First, such objects must exhibit linear, constant velocity motion among the four images. Second, the image shape must be consistent with the seeing-broadened point-spread function of the telescope. Third, the brightness of the image must be constant among images (within the photometric uncertainties). Fourth, the rate of motion must be <10 arcsec/h, corresponding to heliocentric distances >10 AU.

The hundreds of faint main-belt asteroids in our images are immediately rejected from consideration on the basis of their rapid angular motion (~30 arcsec/hr). The thousands of cosmic rays present in each CCD image are spatially uncorrelated, photometrically dissimilar and nonstellar in shape; they violate all four selection criteria and are readily rejected. A more serious problem is posed by drift in the centers of light of faint, arcsecond-sized galaxies caused by nearby noise clumps in the sky brightness. These excursions are uncorrelated among images, however, and are typically confined to angular distances comparable to a galaxy radius. At the faintest levels, sky noise itself produces pseudo images (local maxima) that appear to move between consecutive images. These pseudo images are also spatially uncorrelated and easily rejected.

3. RESULTS FROM THE MAUNA KEA SURVEY

Images from the CCD were flattened in real time at the telescope. The images were also sky-subtracted using a spline-fitting algorithm, and coaligned using field stars in preparation for blinking. Blinking was performed by eye while observing. We find the human eye to be a better detector of linearly moving objects than any computerized algorithms, particularly for objects near the photometric limits of the data.

We detected seven slow-moving objects in the course of the Mauna Kea survey. They are 1992 QB_1, 1993 FW, 1993 RO, 1993 RP, 1994 ES_2, 1994 EV_3, and 1994 GV_9. Table 2 presents the apparent magnitudes of the new objects, together with geometric parameters appropriate to the dates of discovery. Although no observational constraint was imposed on the direction of motion, all seven objects moved westwards in the sky, consistent with the retrograde opposition motion expected of distant objects. Astrometry was obtained using stars from the Hubble Space Telescope *(HST)* Guide Star catalogue (Lasker *et al.* 1990); in most cases we found *HST* guide stars in the fields of the moving objects. Where possible, newly detected objects were reobserved on following nights to improve the astrometric arc. Brian Marsden at the Harvard–Smithsonian Center for Astrophysics supplied us with preliminary ephemerides with which we planned follow-up observations in subsequent months.

The effective limiting magnitude of the observations is primarily determined by properties of the telescope, detector, and atmosphere. The importance of the fine seeing atop

TABLE 1. Observed fields.

N	ECL Field	RA(1950)	Dec(1950)	UT Date
1	223	21:32:03.0	00:01:58	93 / Sep / 16
2	83	21:32:56.8	-14:32:17	92 / Aug / 30
3	224	21:33:56.0	-14:28:03	93 / Sep / 17
4	84	21:36:42.3	-14:13:49	92 / Aug / 29
5	230	21:45:10.6	-13:31:44	93 / Sep / 14
6	232	21:48:54.4	-13:12:31	93 / Sep / 16
7	233	21:50:46.2	-13:02:51	93 / Sep / 17
8	238	22:00:03.0	-12:13:39	93 / Sep / 13
9	239	22:01:53.9	-12:03:40	93 / Sep / 15
10	242	22:07:26.2	-11:33:27	93 / Sep / 17
11	246	22:14:53.1	-10:52:30	93 / Sep / 16
12	248	22:18:27.7	-10:31:46	93 / Sep / 15
13	96	22:21:09.0	-10:15:51	92 / Aug / 30
14	255	22:31:14.7	-09:17:58	93 / Sep / 14
15	266	22:51:11.7	-07:18:24	93 / Sep / 15
16	271	23:00:13.2	-06:22:49	93 / Sep / 13
17	107	23:01:04.8	-06:16:47	92 / Aug / 29
18	282	23:20:00.6	-04:18:20	93 / Sep / 14
19	115	23:29:49.8	-03:14:45	92 / Aug / 30
20	299	23:50:31.5	-01:01:39	93 / Sep / 14
21	300	23:52:19.2	-00:49:59	93 / Sep / 13
22	123	23:58:32.3	-00:08:50	92 / Aug / 30
23	125	00:05:49.0	00:37:56	92 / Aug / 30
24	330	00:46:29.2	04:59:28	93 / Sep / 15
25	331	00:48:18.8	05:11:00	93 / Sep / 17
26	333	00:51:58.0	05:34:00	93 / Sep / 15
27	339	01:02:58.4	06:42:32	93 / Sep / 13
28	340	01:04:48.8	06:53:52	93 / Sep / 16
29	341	01:06:39.4	07:05:12	93 / Sep / 13
30	342	01:08:30.1	07:16:31	93 / Sep / 16
31	357	09:58:41.3	12:20:58	94 / Mar / 13
32	358	10:00:37.7	12:10:32	94 / Mar / 11
33	124	10:30:20.4	09:23:23	93 / Mar / 25
34	125	10:32:14.8	09:12:07	93 / Mar / 26
35	126	10:34:08.3	09:00:57	93 / Mar / 27
36	376	10:35:03.1	08:55:33	94 / Mar / 13
37	127	10:36:01.8	08:49:47	93 / Mar / 28
38	378	10:38:49.5	08:33:08	94 / Mar / 11
39	133	10:47:19.1	07:42:01	93 / Mar / 25
40	146	11:11:31.3	05:12:06	93 / Mar / 26
41	147	11:13:22.3	05:00:25	93 / Mar / 27
42	397	11:14:15.9	04:54:47	94 / Mar / 15
43	155	11:28:06.6	03:26:29	93 / Mar / 28
44	461	11:29:03.0	03:20:46	94 / Apr / 14
45	462	11:30:50.6	03:08:58	94 / Apr / 15
46	406	11:30:50.7	03:08:58	94 / Mar / 13
47	407	11:32:40.7	02:57:08	94 / Mar / 11
48	162	11:40:56.6	02:03:47	93 / Mar / 25
49	476	11:56:27.0	00:23:06	94 / Apr / 15
50	478	12:00:05.8	-00:00:36	94 / Apr / 13
51	173	12:01:01.5	-00:06:38	93 / Mar / 26
52	174	12:02:50.9	-00:18:28	93 / Mar / 27
53	430	12:14:39.4	-01:35:12	94 / Mar / 15
54	486	12:14:39.4	-01:35:12	94 / Apr / 14
55	186	12:24:41.4	-02:40:07	93 / Mar / 28
56	439	12:31:01.3	-03:20:52	94 / Mar / 14
57	192	12:35:35.3	-03:50:06	93 / Mar / 25
58	500	12:40:07.2	-04:19:03	94 / Apr / 13
59	446	12:43:45.7	-04:42:12	94 / Mar / 11
60	447	12:45:35.1	-04:53:45	94 / Mar / 15
61	200	12:50:10.7	-05:22:46	93 / Mar / 26
62	452	12:54:42.2	-05:51:08	94 / Mar / 11
63	456	13:02:00.8	-06:36:36	94 / Mar / 14
64	458	13:05:40.4	-06:59:09	94 / Mar / 14
65	459	13:07:30.3	-07:10:24	94 / Mar / 11
66	460	13:09:20.3	-07:21:36	94 / Mar / 13
67	211	13:10:15.3	-07:27:10	93 / Mar / 25
68	212	13:12:06.7	-07:38:32	93 / Mar / 27
69	518	13:13:00.0	-07:43:24	94 / Apr / 15
70	521	13:20:21.3	-08:28:11	94 / Apr / 13
71	222	13:30:30.5	-09:27:38	93 / Mar / 25
72	537	13:49:58.0	-11:19:04	94 / Apr / 14
73	547	14:08:41.0	-12:59:25	94 / Apr / 15
74	570	14:52:31.4	-16:30:37	94 / Apr / 14
75	573	14:58:19.9	-16:55:36	94 / Apr / 15
76	576	15:04:09.8	-17:19:57	94 / Apr / 14
77	577	15:06:06.7	-17:27:58	94 / Apr / 14
78	579	15:10:00.0	-17:43:39	94 / Apr / 13

TABLE 2. Physical parameters of trans-Neptunian objects.

Name	R [AU] (1)	Δ[AU] (2)	α[deg] (3)	m_R (4)	H_R (5)	D [km] (6)	Discovery Date (7)	Telescope (8)	Reference (9)
1992 QB_1	40.89	39.95	-0.6	22.8	6.62	283	1992 08 30	UH 2.2 m	Jewitt & Luu 1992
1993 FW	42.15	41.15	0.0	22.8	6.60	286	1993 03 28	UH 2.2 m	Luu & Jewitt 1993a
1993 RO	32.32	31.32	0.1	23.2	8.14	139	1993 09 14	UH 2.2 m	Jewitt & Luu 1993b
1993 RP	35.37	34.43	-0.6	24.5	8.96	96	1993 09 15	UH 2.2 m	Luu & Jewitt 1993c
1993 SB	33.15	32.15	-0.2	22.7	7.51	188	1993 09 16	UH 2.2 m	Williams *et al.* 1993
1993 SC	34.45	33.45	-0.1	21.7	6.36	319	1993 09 17	UH 2.2 m	Williams *et al.* 1993
1994 ES_2	45.75	44.79	0.3	24.5	7.87	159	1994 03 13	UH 2.2 m	Jewitt & Luu 1994a
1994 EV_3	44.50	43.60	-0.6	23.3	6.75	267	1994 03 13	UH 2.2 m	Luu & Jewitt 1994a
1994 GV_9	42.18	41.33	0.7	23.1	6.77	264	1994 04 15	UH 2.2 m	Jewitt & Chen 1994a
1994 JS	36.54	35.54	-0.2	22.4	6.78	263	1994 05 11	CTIO 1.5 m	Luu & Jewitt 1994b
1994 JV	35.25	34.33	0.7	22.4	6.86	254	1994 05 13	CTIO 1.5 m	Jewitt & Luu 1994b
1994 JQ_1	43.42	42.48	0.5	22.4	5.97	382	1994 05 11	INT 2.5 m	Irwin *et al.* 1994a
1994 JR_1	35.26	34.28	-0.4	22.5	7.00	238	1994 05 12	INT 2.5 m	Irwin *et al.* 1994a
1994 TB	31.72	30.79	0.5	21.5	6.45	306	1994 10 02	UH 2.2 m	Jewitt & Chen 1994b
1994 TG	42.25	41.26	0.1	23	6.75	266	1994 10 03	UH 2.2 m	Chen *et al.* 1994
1994 TG_2	41.53	40.67	0.6	24	7.75	168	1994 10 08	NTT 3.5 m	Hainaut 1994
1994 TH	40.94	39.94	0.1	23	6.89	249	1994 10 03	UH 2.2 m	Jewitt *et al.* 1994

Notes (1) Heliocenric distance at the time of discovery. (2) Geocentric distance at the time of discovery. (3) Phase angle. (4) Apparent red magnitude. (5) Magnitude reduced to $R = \Delta = 1$ AU and $\alpha = 0°$ (see §4.1). (6) Effective circular diameter computed assuming red geometric albedo $p_R = 0.04$. (8) UH = University of Hawaii, CTIO = Cerro Tololo Inter-American Observatory, INT = Isaac Newton Telescope, NTT = New Technology Telescope.

Mauna Kea should not be underestimated. On a given object, with a fixed integration time, sky brightness, quantum efficiency, and filter, the signal-to-noise ratio obtained varies as $S/N \propto D/\theta$, where D is the telescope diameter and θ is the seeing. For example, our $D=2.2$ m telescope operated with seeing $\theta=0.7$ arcsec equals a 4 m telescope at a site with $\theta=1.3$ arcsec. As a further example of this, we remark that 1993 RP and 1994 ES_2 are both fainter ($m_R \sim 24.5$) than was P/Halley upon recovery with the Palomar 5 m telescope in 1982 ($m_R \sim 24.3$; Jewitt & Danielson 1984). Thus, our moderate-sized telescope is highly optimized for the present deep imaging survey.

We empirically determined the effective limiting magnitude of our survey by creating artificial trans-Neptunian objects in the raw data and then searching for them by blinking. The objects were created using IRAF's ARTDATA package, and added to blink sequences with seeing profiles appropriate to each image and effective angular speeds 3.2 arcsec per hour (corresponding to a circular orbit at $R=40$ AU). This experiment was conducted so that the measurer had no prior knowledge of the location of the artificial moving object, to eliminate the possibility of bias. Artificial objects with apparent red magnitudes $m_R \leq 24.5$ were consistently detected, while those with $m_R \geq 25.2$ were never detected. Thus, the detection probability was approximated by a ramp function falling from 100% at magnitude 24.5 to 0% at 25.2. We note that images of the two objects detected at $m_R=24.5$ (1993 RP and 1994 ES_2) were clear and unambiguous, consistent with the adopted detection probability function.

4. DISCUSSION

The following discussion is directed to the seven objects discovered in the Mauna Kea survey. Additional objects have been reported based on observations taken at La Palma (Spain) and in Chile. Since these observations had a different limiting sensitivity and areal coverage, it is appropriate to separate them in the following statistical analysis. The additional objects are listed in Table 2 and discussed in Sec. *4.5*.

4.1 Photometry and Sizes

The albedos of the trans-Neptunian objects are unknown. Indirect evidence for low albedo is provided by the Centaurs 2060 Chiron and 5145 Pholus, which may both have originated in the trans-Neptunian region (cf. Fernandez 1980; Duncan *et al.* 1988) and which appear to have surfaces that are dark (Davies *et al.* 1993; Campins *et al.* 1994). Likewise, the albedos of the short-period comets are $\sim 0.04 \pm 0.01$ (e.g., Jewitt 1991). To convert the apparent magnitudes and distances to effective radii, a [m], we employ a comet-like geometric albedo $p_R=0.04$ (e.g., Jewitt 1991) and the equation

$$p_R \Phi(\alpha) a^2 = 2.25 \times 10^{22} R^2 \Delta^2 10^{0.4(m_{\rm sun} - m_R)}, \quad (1)$$

in which R [AU] and Δ [AU] are the heliocentric and geocentric distances, α (deg) is the phase angle and $m_{\rm sun}=-27.1$ is the red magnitude of the sun. The phase function $\Phi(\alpha)$ is computed using the "H,G" formalism of Bowell *et al.* (1989) with phase parameter $G=0.15$ as would be appropriate for a dark surface. The results are insensitive to the choice of phase function since all the phase angles in Table 2 are $<1°$ and the phase corrections are typically smaller than the photometric uncertainties.

The derived diameters are listed in Table 2. It may be noticed that the observed objects fall in the diameter range $96 \leq D \leq 380$ km, with no pronounced excess of small objects. This is in apparent contrast with many natural size distributions (e.g., the fragments of impact-shattered rock (Fujiwara *et al.* 1989) or the distribution of the main-belt asteroids (Tedesco 1989), in which small objects are overabundant compared to large ones. We return to this point in Sec. *4.3*.

TABLE 3. Orbital elements of trans-Neptunian objects.

Name (1)	a [AU] (2)	e (3)	i [deg] (4)	Ω [deg] (5)	ω [deg] (6)	Epoch (7)	Source (8)
1992 QB_1	43.84	0.070	2.2	15.69	358.7	1993 Aug 01.0	MPC22594
1993 FW	43.87	0.040	7.7	9.3	187.2	1994 Feb 17.0	MPC23240
1993 RO	39.70	0.20	3.7	184.5	170.3	1994 Sep 05.0	MPEC 1994-R06
1993 RP	35.37	0[a]	2.8	180.6	192.1	1993 Sep 10.0	MPEC 1993-V05
1993 SB	39.42	0.32	1.9	79.0	354.8	1994 Sep 05.0	MPEC 1994-S06
1993 SC	39.50	0.18	5.2	317.0	354.6	1994 Sep 05.0	MPEC 1994-Q04
1994 ES_2	45.75	0[a]	1.1	3.4	154.8	1994 Mar 29.0	MPEC 1994-H03
1994 EV_3	44.50	0[a]	1.6	178.9	19.6	1994 Mar 29.0	MPEC 1994-H04
1994 GV_9	42.18	0[a]	0.1	325.0	208.5	1994 Apr 18.0	MPEC 1994-L06
1994 JS	36.54	0[a]	15.4	180.0	56.3	1994 May 08.0	MPEC 1994-L02
1994 JV	35.25	0[a]	18.1	178.0	28.1	1994 May 08.0	MPEC 1994-L03
1994 JQ_1	43.31	0[a]	3.8	183.6	25.7	1994 May 08.0	MPEC 1994-L05
1994 JR_1	35.26	0[a]	3.8	99.7	143.8	1994 May 08.0	MPEC 1994-L04
1994 TB	31.72	0[a]	10.2	41.9	309.7	1994 Sep 25.0	MPEC 1994-T02
1994 TG	42.25	0[a]	6.8	353.0	15.5	1994 Sep 25.0	MPEC 1994-T03
1994 TG_2	41.53	0[a]	3.9	359.3	352.8	1994 Sep 25.0	MPEC 1994-T14
1994 TH	40.94	0[a]	16.1	356.5	12.1	1994 Sep 25.0	MPEC 1994-T04

Notes
a = circular orbit assumed
5 = Argument of latitude (epoch 2000)
6 = Node (epoch 2000)
8 MPC = Minor Planet Circular, MPEC = Minor Planet Electronic Circular

4.2 Statistics (Simplified)

We wish to understand the constraints placed on the size and radial distance distributions of the trans-Neptunian bodies by the present survey. Therefore, in Sec. *4.3* we consider bias effects inherent in the present survey. However, a crude but sturdy estimate of the large-diameter population is possible and useful. Based on this survey, the surface density of objects brighter than $m_R=25$ is $\Sigma=7/1.2\sim6$ per sq deg. The detected objects have diameters $D\geqslant100$ km (Table 2) and heliocentric distances in the range $30\leqslant R\leqslant50$ AU. Substantially smaller and/or more distant objects would not be recorded in the present data. The near-coplanarity of the orbits (Table 3) suggests strongly that the trans-Neptunians are part of a belt or disk rather than members of an isotropic distribution. The most inclined trans-Neptunian from this survey has orbital inclination $i=8$ deg (Table 2). Accordingly, we take the area of the sky occupied by trans-Neptunians as a band, 16 deg thick by 360 deg around the ecliptic, for a total area $A=5760$ sq deg. The number of trans-Neptunians having $D\geqslant100$ km and $30\leqslant R\leqslant50$ AU is then $N\sim\Sigma A\sim35\,000$. For comparison, the number of main-belt asteroids having $D\geqslant100$ km is ~230 (Tedesco 1989). Even allowing that our estimate of the trans-Neptunian population is uncertain by a factor of several, it is clear that these distant objects vastly outnumber the main-belt asteroids of comparable size. The total mass of 35 000 spheres of 100 km diameter each having density 1000 kg m^{-3} is $\mathcal{M}\sim1.8\times10^{22}$ kg$\sim0.003\mathcal{M}_E$, where $1.\mathcal{M}_E=6\times10^{24}$ kg is the mass of the earth. Considerable mass could be hidden in smaller objects, or in larger objects too rare to be detected in the present survey. Note that the inferred mass is small compared to the upper limit $\mathcal{M}\sim1\mathcal{M}_E$ inferred dynamically (Hamid *et al.* 1968; Yeomans 1986; Hogg *et al.* 1991) and comparable to the mass required if the short-period comets are derived from the trans-Neptunian Kuiper Belt (Duncan *et al.* 1988; Ip & Fernandez 1991; Duncan & Quinn 1993).

4.3 Statistics (Detailed)

The maximum distance to which a given object may be detected in reflected light is a function of the area×albedo product of the object. Large objects may be detected in a larger volume than small ones, leading to an overrepresentation of large objects in the sky-plane surface density. In other words, the present survey is "flux-limited" rather than "volume-limited," and we must apply a model-dependent correction for the resulting bias in the data. The necessary correction depends on the geometry of the Kuiper belt, and on the sensitivity cutoff of the survey.

The qualitative features of the flux-limited bias may be deduced from a simple model in which the Kuiper Belt is approximated by a plane-parallel sided disk with a central hole of radius R_0, and perpendicular thickness $2H$. We suppose that the flux density of sunlight scattered back to Earth from a single object of radius a (km) is given by

$$f_\nu=\frac{Ka^2}{R^2\Delta^2}, \tag{2}$$

where R [AU] is the heliocentric distance and Δ [AU] is the geocentric distance. Comparing Eqs. (1) and (2), we see that constant $K=[p_R\Phi(\alpha)f_{\rm sun}]/2.25\times10^{22}$, with $f_{\rm sun}$ [W m^{-2} Hz^{-1}] being the flux density of solar radiation at the orbit of earth. For observations at small phase angle, $\Delta=R-1$, and for $R\gg1$, we may put $\Delta\sim R$ to a good level of approximation, giving $f_\nu\sim Ka^2R^{-4}$. For illustrative purposes, we assume that the differential size distribution is a power law

$$n(a)da=\Gamma a^{-q}\,da, \tag{3}$$

where $n(a)da$ is the number density of objects in the radius range a to $a+da$, and Γ and q are constants. The survey detection probability is taken to be 100% for flux densities $f\geqslant f_{\rm lim}$ and 0% otherwise. We define a_0 as the radius of the smallest detectable body at $R=R_0$, so that $a_0=(f_{\rm lim}/K)^{1/2}R_0^2$.

An object of radius $a>a_0$ will be visible to a distance $R_1>R_0$. The volume contained in $R_0\leqslant R\leqslant R_1$ is $V=2\pi H(R_1^2-R_0^2)$. Therefore, the number of objects of radius a to $a+da$ contained in this volume is

$$N(a)da=2\pi H\Gamma R_0^2 a^{-q}\left(\frac{a}{a_0}-1\right)da. \quad (4)$$

Equation (4) has two important features. First, the equation has a maximum at

$$a_{\max}=\left(\frac{q}{q-1}\right)a_0, \quad (5)$$

indicating that the apparent surface density of objects drawn from an intrinsic power law distribution peaks, not at the smallest observable size, but at $q/(q-1)$ times that size. Second, for $a/a_0\gg 1$, we see that $N(a)da\propto a^{1-q}$, so that the flux-limited distribution is flatter than the intrinsic (volume-limited) distribution by one power of a at large sizes. While clearly oversimplified, this analytic model serves to show that the apparent distribution of object sizes should be flatter than the intrinsic distribution, and should have a maximum at sizes larger than the intrinsically most abundant size in the distribution.

To more conveniently explore the relation between the observed surface density of trans-Neptunian objects and the parameters of the presumed Kuiper disk, we constructed a Monte Carlo simulation program. The program does the following:

(1) Randomly selects a radius in the range $a_0\leqslant a\leqslant a_1$, according to the desired size distribution,

(2) Randomly selects a heliocentric distance in the range $R_0\leqslant R\leqslant R_1$, according to the desired heliocentric distribution. We adopt a power-law, in which the number density varies as R^{-p}, with $p=$constant.

(3) Computes the reflected flux, f_v, from the object according to Eq. (2),

(4) compares the reflected flux with the limiting sensitivity of the survey to decide whether the object is "observable" or not. The empirical detection probability (Sec. 3) is employed. If the object falls within the observable domain of the survey, its parameters (size, distance, magnitude) are recorded for later study.

(5) Repeats the above steps until a sample of the required size has been accumulated.

Figure 2 shows a Monte Carlo simulation obtained using this prescription. The top curve shows the intrinsic size distribution (here taken to be a $q=2$ power law) while the bottom shows the apparent size distribution derived from it. The radial density distribution is assumed to vary as R^{-2}. The inner edge is placed at $R_0=32$ AU, to agree with the smallest orbits found to date (1993 RO and 1994 TB: Table 2), while the outer radius is effectively infinite (the model results are insensitive to the outer radius provided it is $\gg R_0$). In this geometry, the smallest detectable object at the inner edge of the disk has radius $a=27$ km but the apparent sky-plane surface density peaks at $a\sim 50$ km. The figure shows that the apparent density falls more slowly with increasing radius than does the intrinsic density. Thus, the simulation exhibits

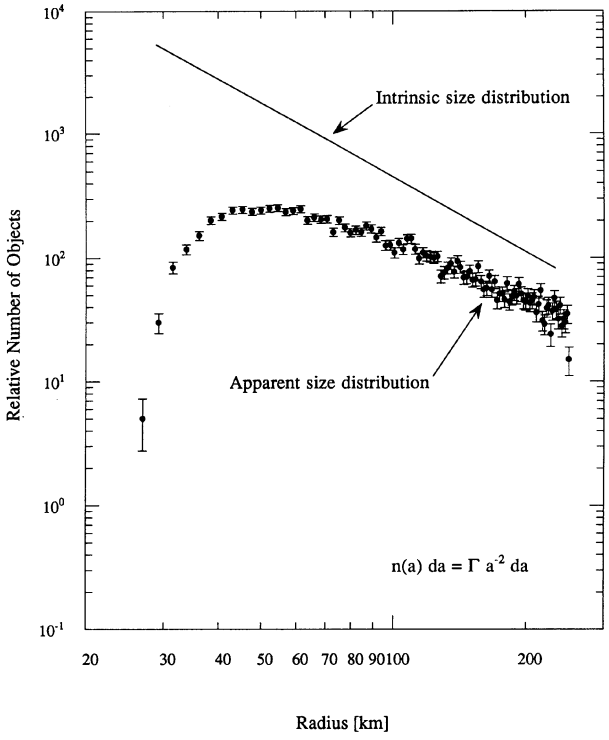

FIG. 2. Intrinsic and apparent number densities of trans-Neptunians are compared, to show the effects of bias in the present observations. The upper curve refers to an intrinsic $q=2$ power law size distribution of Kuiper Belt objects, with an assumed inner belt radius $r_0=32$ AU. The total number density in the belt is taken to vary with heliocentric distance as R^{-p} with $p=2$. The points were computed using the Monte Carlo simulation described in the text, with $N=10^4$ particles. The flattening and fall off of the apparent simulation near radii ~ 50 km are observational artifacts resulting from the flux-limited nature of the survey. The intrinsic and apparent curves have been displaced vertically for clarity.

the basic features outlined on the basis of analytical approximations above.

In Fig. 3 we compare three Monte Carlo simulations in which the intrinsic size distribution follows Eq. (3) with indices $q=1$, 2, and 3. The upper and lower limit radii are $a_0=27$ km and $a_1=250$ km. The radial density distribution is again assumed to vary as R^{-2} for all $R\geqslant R_0=32$ AU. The limiting sensitivity is taken to be a ramp, in which the probability of detection of an object decreases smoothly from 100% at $m_R=24.5$ to 0% at $m_R=25.2$. The discovered trans-Neptunians are also plotted for comparison. Figure 3 confirms that geometrical and observational biases in the survey data lead to a flattening of the apparent size distribution relative to the intrinsic distribution. For instance, the middle curve ($q=2$) predicts an apparent surface density which varies by only a factor of 2 for radii from ~ 35 to ~ 100 km. The intrinsic surface density varies by a factor $(100/35)^2\sim 8$ over the same range. This provides a natural explanation for the absence of a strong concentration of detected objects at small sizes. Figure 3 suggests that distributions with $q=3$ and larger are too steep to fit the survey data. We tentatively conclude that the size distribution of the trans-Neptunians is

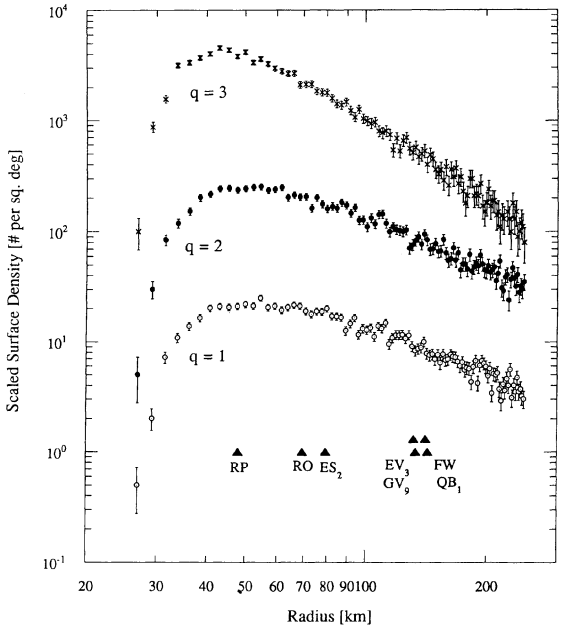

FIG. 3. Monte Carlo simulations of a trans-Neptunian belt, showing the apparent surface density of detected objects as a function of the radius. The total number density in the belt is taken to vary with heliocentric distance as R^{-2}. The three curves show size distributions of the form $n(a)da = \Gamma a^{-q}\,da$, with Γ constant and $q=3$ (top curve), $q=2$ (middle) and $q=1$ (bottom curve). Each simulation employed 10^4 points; the error bars show uncertainties within the binned data. The curves have been displaced vertically for clarity. The radii of the seven trans-Neptunians detected in the present survey are marked by filled triangles and labelled for comparison.

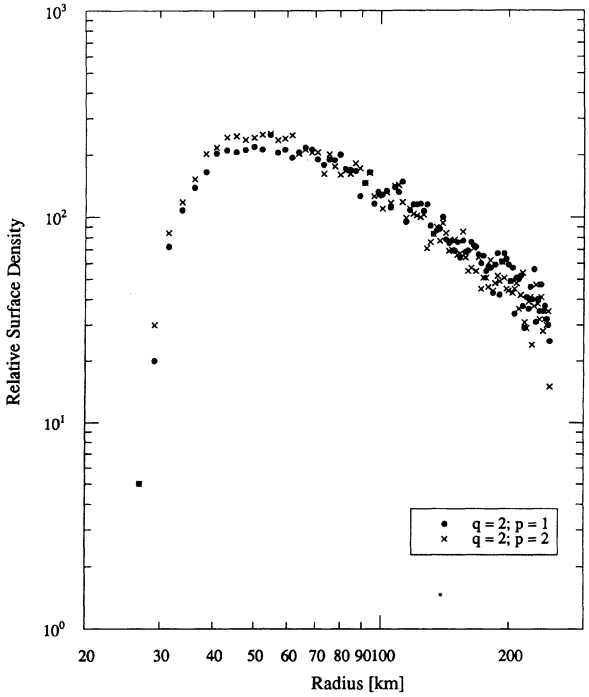

FIG. 4. Effect of the disk radial gradient is shown. Objects in both models were assumed to obey a power-law size distribution with $q=2$. Radial indices $p=1$, and $p=2$ are plotted. Evidently, the apparent surface density is weakly dependent on the radial index.

flatter than that of the main-belt asteroids, for which $q\sim3$ (Tedesco 1989).

The effect of the radial density gradient in the trans-Neptunian disk is shown in Fig. 4, where models having radial index $p=1$ and $p=2$ are shown. Figure 4 shows that the apparent surface density is only weakly dependent on the radial structure of the disk. Our physical interpretation is that the present survey is highly biased towards objects at the inner edge of the disk, and allows only a thin inner strip of the disk to be studied, roughly from the inner edge (32 AU) to about 50 AU. Radial variations across this thin strip are small.

Figure 5 shows the distribution of heliocentric distances of the detected objects for a power-law model having $p=q=2$. The trans-Neptunians are explicitly marked. The heliocentric distances of detectable model objects are concentrated towards the inner edge of the belt, as a result of both the radial density gradient and the near R^{-4} dependence in Eq. (2). Likewise, the trans-Neptunians cluster at distances $R\leqslant45$ AU, but show a deficit in $30\leqslant R\leqslant40$ AU relative to the model histogram. Erosion (or "sculpting") of the inner edge of the belt (cf. Gladman & Duncan 1990; Levison 1991; Levison & Duncan 1993; Holman & Wisdom 1993) will cause the density of objects in the observable inner region to fall considerably below the power law prevalent further out. A view of the ecliptic plane for the particular model used in Fig. 5 is shown in Fig. 6. Objects that satisfy the detection criteria of the Mauna Kea survey are enclosed in circles. Clearly, the present survey is highly biased to objects at the inner edge of the belt.

Results obtained assuming a power-law size distribution of trans-Neptunian objects are nonunique, and we have experimented with other size distributions in the simulations. Agglomerative growth by gravitational instability gives rise to a preferred initial size, which may vary only weakly with heliocentric distance (Goldreich & Ward 1973; Yamamoto & Kosaza 1988; Bailey 1994). Collisions in the inner belt ought to produce a spread of diameters, but at distances $R\geqslant50$ AU, the collision time becomes longer than the age of the solar system and a nearly monodispersed size distribution might be preserved. We have therefore also computed Monte Carlo models using Gaussian size distributions for the trans-Neptunian objects. Within the uncertainties, we can indeed find Gaussian size distributions that match the data as well as the power laws shown in Fig. 3. The success of both power-law and Gaussian models serves primarily to highlight the insufficiencies of the available data. Probably the strongest conclusion allowed by the data is that power law distributions steeper than $q=3$ predict more small objects than are observed.

The graphs and remarks above refer to particular choices of model parameters that are open to legitimate question. It is not our intent to argue that specific parameters can be uniquely identified from the presently available data, but rather to show that the basic observational properties of the trans-Neptunian objects are consistent with the presence of a

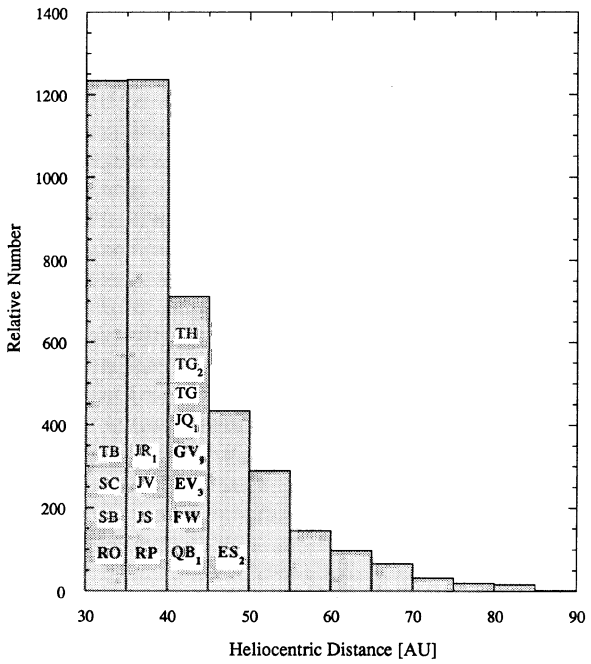

FIG. 5. Histogram of the heliocentric distances of trans-Neptunian objects "detected" according to the Monte Carlo simulation described in Sec. *4.3*. The model assumes a smooth disk with radial gradient $p=2$, inner edge at 32 AU and objects distributed according to a power law of index $q=2$. For comparison, actual detected trans-Neptunians are labelled. Those in bold type are from the Mauna Kea survey while those in plain type are from independent surveys with different limiting magnitudes (see Table 2). The deficit observed at $R \leq 40$ AU presumably results from clearing of the inner edge of the belt by Neptune.

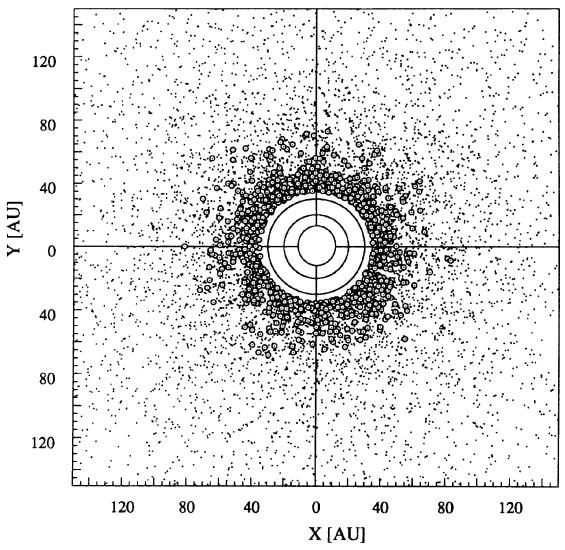

FIG. 6. Plan view of the Monte Carlo simulation in Fig. 5. Objects generated by the simulation are plotted as points, while objects that satisfy the detection criteria of the Mauna Kea survey are marked as circles.

belt. Future observations of large numbers (hundreds?) of trans-Neptunians will reveal the true size and distance distributions of these objects, and will permit detailed comparisons with published models. We note that Gaussian or weak (e.g., $q=2$) power-law distributions may not accommodate the large number of $D \sim 1$ to 10 km sized objects that are required if the trans-Neptunian region is the source of the short period comets. We are attempting a direct assessment of the small body population using deep imaging from the Keck 10 m telescope.

4.4 Comparison with Other Surveys

In addition to the seven trans-Neptunians identified in this survey of 1.2 sq deg to magnitude 25, a further ten distant objects have been reported in separate, less deep and (as of yet) unpublished surveys (Williams *et al.* 1993; Jewitt & Luu 1994a, b; Luu & Jewitt 1994a, b; Irwin *et al.* 1994a, b; Jewitt & Chen 1994b; Chen *et al.* 1994; Hainaut 1994; Jewitt *et al.* 1994). Parameters of these objects are included in Tables 2 and 3.

Figure 7 shows the cumulative surface density derived from these and other surveys, as a function of the limiting red magnitude (Table 4). The present survey yields the points at $m_R=23$, 24, and 25 (cumulative counts of 2, 5, and 7 objects in 1.2 sq deg, respectively). Uncertainties and upper limits to the surface densities as plotted in the figure were computed assuming a Poisson counting distribution. The plotted error bars correspond to $\pm 1\sigma$, while upper limits correspond to 99.5% confidence (approximately 3σ). We include Pluto (Tombaugh 1961) as a trans-Neptunian object even though its elliptical orbit has a perihelion inside the orbit of Neptune. Unfortunately, its placement in Fig. 7 is problematic. The albedo of its ice-covered surface is of order 0.6, or 15 times larger than the adopted albedo of the other trans-Neptunians. The presence of surface ice is presumably an artifact of Pluto's gravity, which is able to retain sublimated molecules that would promptly escape from smaller bodies. If Pluto were darkened to albedo 0.04, it would fade by 3 mag, and in the process would have converted Tombaugh's data point in Fig. 7 into an upper limit.

A few points are obvious from Fig. 7. First, our previous CCD survey of 0.34 sq deg to $m_R=24$ (Paper 1) failed to detect trans-Neptunians because the area examined was too small. Second, Levison & Duncan (1990) detected no trans-Neptunians in a survey of 4.9 sq deg, and concluded that the surface density to $m_R=22$ was less than 1 per sq deg at the 99% confidence level. This is slightly surprising in view of the detection of 1993 SC at $m_R=21.7$ (Table 2) in a survey of only ~0.5 sq deg, but the implied disagreement in surface densities is not large. Third, a very stringent limit to the cumulative surface density at $m_R \sim 19.5$ is placed by Kowal (1989).

TABLE 4. Published surveys of trans-Neptunians.

Reference	m_R limit (1)	Area [sq. deg] (2)	# detected (3)	Σ [deg^{-2}] (4)
Tombaugh (1961)	16.8	1530	1	6.5×10^{-4}
Kowal (1990)	19.5	6400	0	$<8.6 \times 10^{-4}$
Luu & Jewitt (1988)	20.0	297	0	$<1.9 \times 10^{-2}$
Levison & Duncan (1990)	22.0	4.9	0	<1.1
Luu & Jewitt (1988)	24.0	0.34	0	<16
This Work	25.0	1.2	7	6

Notes (1) Effective limiting magnitude (R band). (2) Area surveyed. (3) Number of objects detected. (4) Resulting cumulative surface density.

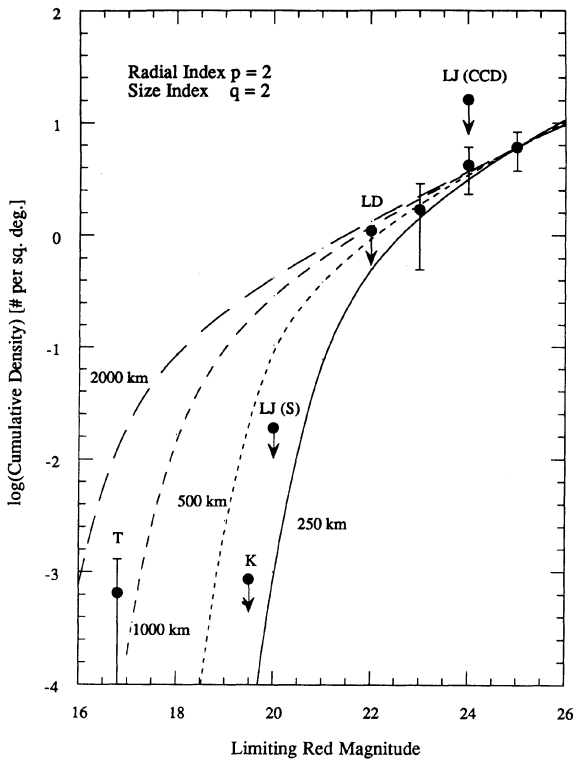

FIG. 7. Cumulative surface density constraints on the trans-Neptunian population derived from selected ecliptic surveys as a function of the limiting magnitude of each survey. In the figure, T=Tombaugh (1961), K=Kowal (1989), LD=Levison & Duncan (1990), while LJ (Schmidt) and LJ (CCD) are two limits from Luu & Jewitt (1988). Arrows [for K, LD, LJ (Schmidt), and LJ (CCD)] denote 99.5% confidence upper limits. Unmarked data points are derived from the present Mauna Kea observations. Error bars (for T and this work) denote 1σ uncertainties computed from Poisson counting statistics. The curves denote disk models having radial index $p=2$ and power-law size distribution index $q=2$. The models are normalized to the $m_R=25$ datum. The maximum radius in each model is marked.

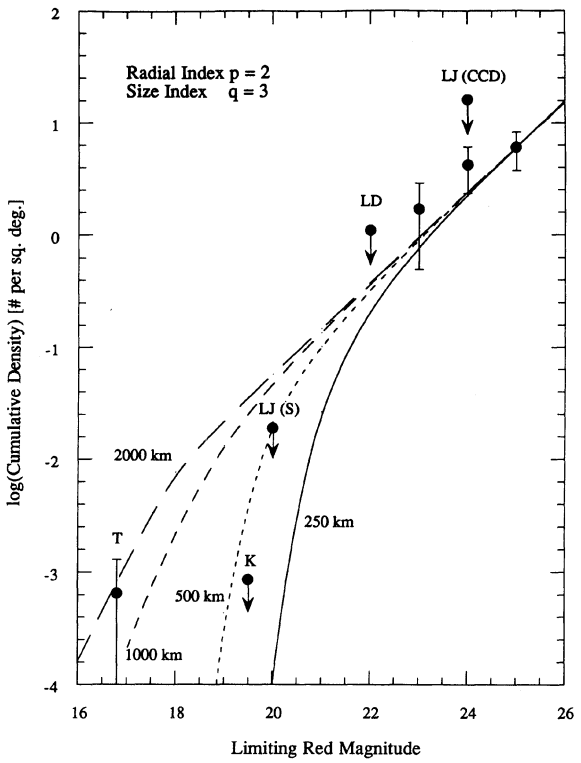

FIG. 8. Same as Fig. 7, but the model curves are computed using differential size distribution index $q=3$.

We applied the belt model from Sec. *4.3* to the combined data of Fig. 7. Lines in Fig. 7 show models having differing values of maximum radius, a_1, as marked. We find that the qualitative features of Fig. 7 are matched by $q=2$ power laws truncated at $a_1\sim300$ km, or about twice the size of the largest objects in Table 2. This upper limit size is forced primarily by the limits from Kowal (1989) and Paper I at $m_R=19.5$ and at $m_R=20$, respectively. The maximum size is only weakly dependent on the power law size index, as may be seen by comparing Fig. 7 with Fig. 8 ($q=2$ in Fig. 7 and $q=3$ in Fig. 8). In both figures the limits near $m_R\sim19$ to 20 require $a_1\sim300$ km. Pluto is the sole exception to the otherwise good match between the models and the data. Pluto (radius ~1100 km) cannot be fit by models based on power law size distributions of any index, essentially because of the stringent limit at $m_R=19.5$. We tentatively conclude that trans-Neptunians larger than ~300 km radius are depleted relative to power law extrapolations from smaller radii, but that a few larger objects up to and including Pluto, do exist. A general depletion of large bodies would be a natural consequence of the inordinately long timescales for growth in the outer regions of the pre-planetary disk.

The inclination distribution of the short-period comets is plotted in Fig. 9(a) (Marsden 1983). The corresponding distribution for the trans-Neptunians is shown in Fig. 9(b). If the trans-Neptunians are identified with the source region of the short-period comets, we should expect the two histograms in Fig. 9 to be of comparable width. To make a comparison between the inclination distributions, we must first correct for the inclination bias present in the trans-Neptunian survey data. In the ecliptic frame, the latitude of a body following an inclined orbit varies approximately sinusoidally with time while the longitude increases linearly (we neglect the opposition retrograde loop and other complications). The probability that a body having orbital inclination i [rad] will fall in the field of view of a square detector of width h [rad] is

$$P(h,i)=\left(\frac{2}{\pi}\right)\left(\frac{h}{2\pi}\right)\sin^{-1}\left(\frac{h}{2i}\right), \tag{6}$$

assuming that the detector is aimed at ecliptic latitude 0. Since $h/(2i)\ll1$ for most surveys, we may write $P(h,i)\sim h^2/(2\pi i)$, showing that highly inclined orbits are highly discriminated against in surveys with small fields of view. The effect of this inclination bias may be judged from the shaded histogram in Fig. 9(a), in which the short-period comet inclinations have been weighted by the probability function given in Eq. (6). We used $h=0.12°$, as appropriate for the Tektronix 2048 CCD, and normalized to the number

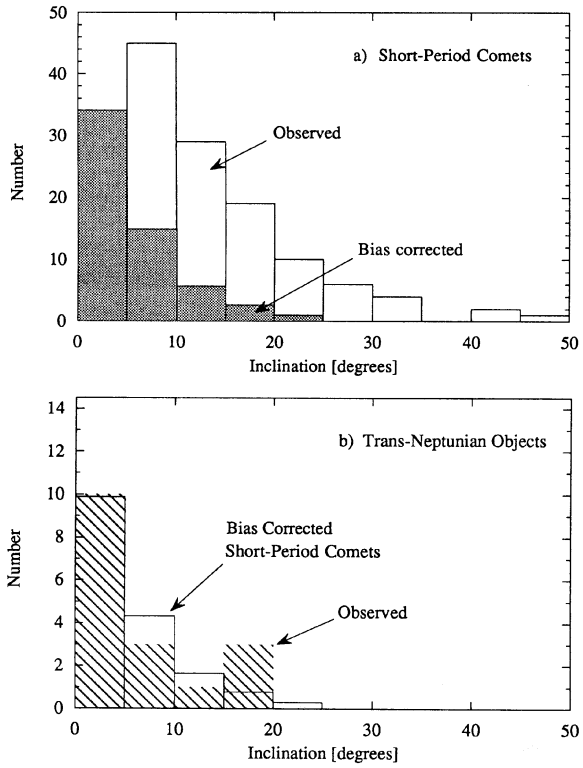

FIG. 9. (a) Inclination distribution of the short-period comets is compared with (b) the corresponding distribution for trans-Neptunians. The shaded histogram in panel (a) shows the effect of including the inclination bias [Eq. (6)] in the short-period comet observations. High inclination comets would be heavily discriminated against if observed using the strategy employed to detect trans-Neptunians. Panel (b) compares the inclination distributions of the trans-Neptunian objects and the bias corrected short-period comets.

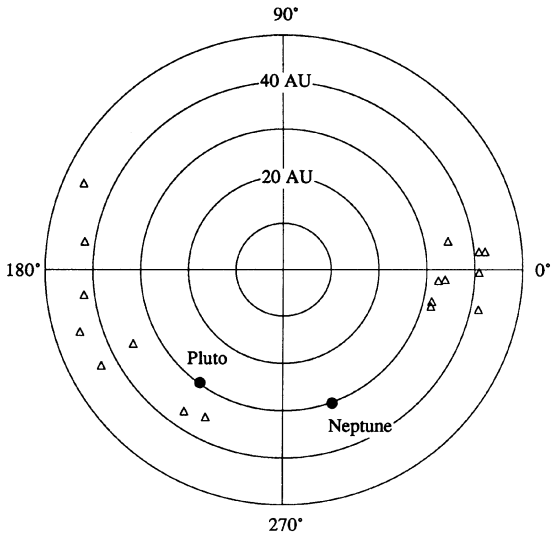

FIG. 10. Polar plot of ecliptic longitude vs heliocentric distance. Small triangles denote the new trans-Neptunian objects while Pluto and Neptune are marked. The nonuniform azimuthal distribution is an artifact of the search strategy employed.

of comets in the 0°–5° bin. Within the uncertainties imposed by the small size of the trans-Neptunian object sample, we find no compelling evidence in Fig. 9(b) for a difference between the comet and trans-Neptunian inclination distributions.

Trans-Neptunians with perihelion distances $\geq$40 AU are likely to be dynamically stable against Neptune perturbations on time scales comparable to, or longer than, the age of the solar system (cf. Levison & Duncan 1993; Holman & Wisdom 1993). While the perihelion distances of most of the trans-Neptunians are not yet well known, it is at least plausible that 1992 QB_1, 1993 FW, 1994 ES_2, EV_3, GV_9, JQ_1, TG, TG_2, and TH (all with $R \geq 40$ AU; see Table 2) are permanent residents of a primordial disk. Conversely, other objects are close enough to the orbit of Neptune that their survival on billion-year time scales is in doubt. Members of the latter group include 1993 RO, RP, SB, SC, and 1994 JS, JV, JR_1, and TB. An initial suggestion that these objects might be stabilized by a 1:1 mean motion resonance with Neptune (i.e., they are Neptune Trojans; Marsden 1993) seems statistically unlikely because all eight objects are beyond the orbit of Neptune (Fig. 10), whereas ~50% of Neptune trojans should appear inside the orbit of the planet at any epoch of observation. However, a trojan origin remains possible for 1994 TB at $R \sim 32$ AU (see Table 2). Alternatively, the $R \leq 40$ AU objects might be in Pluto-like 2:3 mean motion resonances with Neptune (Marsden 1994a). The astrometry of 1993 RO, SB, and SC is particularly well described by 2:3 resonance orbit solutions (Marsden 1994b). As would be expected in this hypothesis, these objects appear at large angular separations from Neptune (Fig. 10), but this is an artifact of yet another observational selection effect caused by our avoidance of the Milky Way, against which Neptune and its vicinity must presently be observed.

The existence of numerous small Plutos ("Plutinos") would complicate the simplistic representation of the trans-Neptunian belt used in Sec. *4.3*. For example, Plutinos would appear nonuniformly distributed in ecliptic longitude in our flux-limited survey, as a result of their aphelion alignment with Neptune. These and other uncertainties prevent an accurate assessment of the number of Plutinos. However, the high rate of detection of these objects and the reasoning of Sec. *4.2* together suggest a population that is at least measured in the thousands (for $D \geq 100$ km). Future astrometric observations will be needed to clarify the dynamical characters of the newly detected objects and provide meaningful and exciting tests of theories of their origin (cf. Malhotra 1993).

5. SUMMARY

(1) We present the results of an optical survey of 1.2 sq deg of the ecliptic to limiting apparent red magnitude 25. The survey is optimized to reveal slow moving objects at large heliocentric distances.

(2) Seven trans-Neptunian objects were discovered in this survey. We and others have discovered an additional ten objects in related, less deep surveys. These new detections constitute strong evidence for a substantial population of bodies

beyond Neptune. While it is still too early to rigorously prove that the new objects are long-lived members of the putative Kuiper Belt (Edgeworth 1949; Kuiper 1951; Duncan *et al.* 1988), this is a plausible interpretation for objects with perihelia $\geq$40 AU. Objects with smaller perihelia (especially 1993 RO, SB, and SC) might be Plutinos, in 2:3 mean motion resonance with Neptune.

(3) We estimate that ~35 000 trans-Neptunian objects with diameters $D \geq 100$ km exist in the $30 \leq R \leq 50$ AU region.

(4) The flat apparent size distribution of the detected trans-Neptunians is partly a result of observational selection in our flux-limited (as opposed to volume-limited) survey. The survey data are compatible with an *intrinsic* inverse-square power law differential size distribution, as well as with flatter power laws and Gaussian distributions. They are incompatible with power-law distributions with indices ≥ 3, suggesting that the size distribution may be flatter than in the main asteroid belt, at least in the 100 to 400 km diameter range. More sensitive observations will be needed to show whether 1 to 10 km sized objects exist in numbers sufficient to replenish the short-period comets.

(5) The cumulative magnitude distribution of trans-Neptunian objects suggests that the size distribution is depleted at radii $\geq$300 km. This might represent the maximum size to which most trans-Neptunian objects could grow in the low density regions of the pre-planetary disk.

(6) The inclination distribution of the trans-Neptunian objects is compatible with the inclination distribution of the short-period comets, once observational selection effects are taken into proper account.

We thank Dave Woodworth and Frank Cheigh for their work as operators on the 88 in. telescope. Brian Marsden helped greatly with interpretation of the astrometry of the new objects and kindly read a draft of this paper. DCJ is grateful for recent support of this work from NASA's Origins of Solar Systems Program. JXL acknowledges support as a Hubble Fellow.

REFERENCES

Bailey, M. E. 1994, in Asteroids, Comets, Meteors 1993, edited by A. Milani, M. Di Martino, and A. Cellino (Kluwer, Dordrecht), pp. 443–459
Bowell, E., Hapke, B., Domingue, D., Lumme, K., Peltoniemi, J, & Harris, A. 1989, in Asteroids II, edited by R. Binzel, T. Gehrels, and M. Matthews (University of Arizona, Tucson), pp. 524–556
Campins, H., Telesco, C., Osip, D., Rieke, G., Reike, M., & Schulz, B. 1994, AJ (submitted)
Chen, J., Jewitt, D. C., & Knopp, G. 1994, Minor Planet Electronic Circular No. 1994-T03 (Oct 08)
Cochran, A. L., Cochran, W. D., & Torbett, M. V. 1991, BAAS 23, 1158
Davies, J., Spencer, J., Sykes, M., Tholen, D., & Green, S. 1993, I.A.U.C. 5698 (Jan 27)
Duncan, M., Quinn, T., & Tremaine, S. 1988, ApJ, 328, L69
Duncan, M. J., & Quinn, T. 1993, in Protostars and Planets III, edited by E. Levy and J. Lunine (University of Arizona, Tucson), pp. 1371–1394
Edgeworth, K. E. 1949, MNRAS, 109, 600
Fernandez, J. A. 1980, MNRAS, 192, 481
Fujiwara, A., Cerroni, P., Davis, D., Ryan, E., Di Martino, M., Holsapple, K., & Housen, K. 1989, in Asteroids II, edited by R. Binzel, T. Gehrels, and M. Matthews (University of Arizona, Tucson), pp. 240–265
Gladman, B., & Duncan, M. 1990, AJ, 100, 1680
Goldreich, P., & Ward, W. 1973, ApJ, 183, 1051
Hainaut, O. 1994, Minor Planet Electronic Circular No. 1994-T14 (Oct 13)
Hamid, S. E., Marsden, B., & Whipple, F. 1968, AJ, 73, 727
Hogg, D. W., Quinlan, G. D., & Tremaine, S. 1991, AJ, 101, 2274
Holman, M., & Wisdom, J. 1993, AJ, 105, 1987
Ip, W.-H., & Fernandez, J. A. 1991, Icarus, 92, 185
Irwin, M., Zytkow, A., Tremaine, S., & Webster, R. 1994a, Minor Planet Electronic Circular No. 1994-K05 (May 26)
Irwin, M., Zytkow, A., Tremaine, S., & Webster, R. 1994b, Minor Planet Electronic Circular No. 1994-K06 (May 26)
Jewitt, D. C., & Chen, J. 1994a, Minor Planet Electronic Circular No. 1994-L06 (Jun 15)
Jewitt, D. C., & Chen, J. 1994b, Minor Planet Electronic Circular No. 1994-T02 (Oct 05)
Jewitt, D. C. 1991, in Comets In The Post-Halley Era, edited by R. Newburn, M. Neugebauer, and J. Rahe (Kluwer, Netherlands), pp. 19–65
Jewitt, D. C., & Danielson, G. E. 1984, Icarus, 60, 435
Jewitt, D. C., & Luu, J. X. 1992, I.A.U.C. 5611 (Sept. 14)
Jewitt, D. C., & Luu, J. X. 1993a, Nature, 362, 730
Jewitt, D. C., & Luu, J. 1993b, I.A.U.C. 5865 (Sept. 18)
Jewitt, D. C. & Luu, J. X. 1994a, Minor Planet Electronic Circular No. 1994-F05 (Mar 22)
Jewitt, D. C., & Luu, J. X. 1994b, Minor Planet Electronic Circular No. 1994-J09 (May 14)
Jewitt, D. C., Chen, J., & Knopp, G. 1994, Minor Planet Electronic Circular No. 1994-T04 (Oct 08)
Kowal, C. 1989, Icarus, 77, 118
Kuiper, G. P. 1951, in Astrophysics, edited by J. A. Hynek (McGraw-Hill, New York), pp. 357–424
Lasker, B., Sturch, C., McLean, B., Russell, J., Jenkner, H., & Shara, M. 1990, AJ, 99, 2019
Levison, H. F. 1991, AJ, 102, 787
Levison, H. F., & Duncan, M. J. 1990, AJ, 100, 1669
Levison, H. F., & Duncan, M. J. 1993, ApJ, 406, L35
Luu, J. X., & Jewitt, D. 1988, AJ, 95, 1256 (Paper I)
Luu, J. X., & Jewitt, D. 1993a, I.A.U.C. 5730 (Mar 29)
Luu, J. X., & Jewitt, D. 1993b, I.A.U.C. 5867 (Sept 20)
Luu, J. X., & Jewitt, D. 1994a, Minor Planet Electronic Circular No. 1994-F04 (Mar 19)
Luu, J. X., & Jewitt, D. 1994b, Minor Planet Electronic Circular No. 1994-J07 (May 13)
Malhotra, R. 1993, Nature, 365, 819
Marsden, B. G. 1983, Catalog of Cometary Orbits (Enslow, New Jersey)
Marsden, B. G. 1993, I.A.U.C. 5865 (Sept. 18)
Marsden, B. G. 1994a, I.A.U.C. 5983 (May 3)
Marsden, B. G. 1994b, I.A.U.C. 6076 (Sep 10)
Tedesco, E. 1989, in *Asteroids II*, edited by R. Binzel, T. Gehrels and M. Matthews (University of Arizona, Tucson), pp. 1090–1138
Tombaugh, C. W. 1961, in Planets and Satellites, edited by G. P. Kuiper and B. M. Middlehurst (University of Chicago, Chicago), pp. 12–30
Tyson, J. A., Guhathakurta, P., Bernstein, G., & Hut, P. 1992, BAAS, 24, 1127
Whipple, F. L. 1964, Proc. Nat. Acad. Sci., 51, 711
Williams, I. P., Fitzimmons, A., & O'Ceallaigh, D. 1993, I.A.U.C., No. 5869 (September 22)
Yamamoto, T., & Kosaza, T. 1988, Icarus, 75, 540
Yeomans, D. K. 1986, in Proc. 20th ESLAB Symp. (ESA SP-250, Heidelberg), pp. 419–425

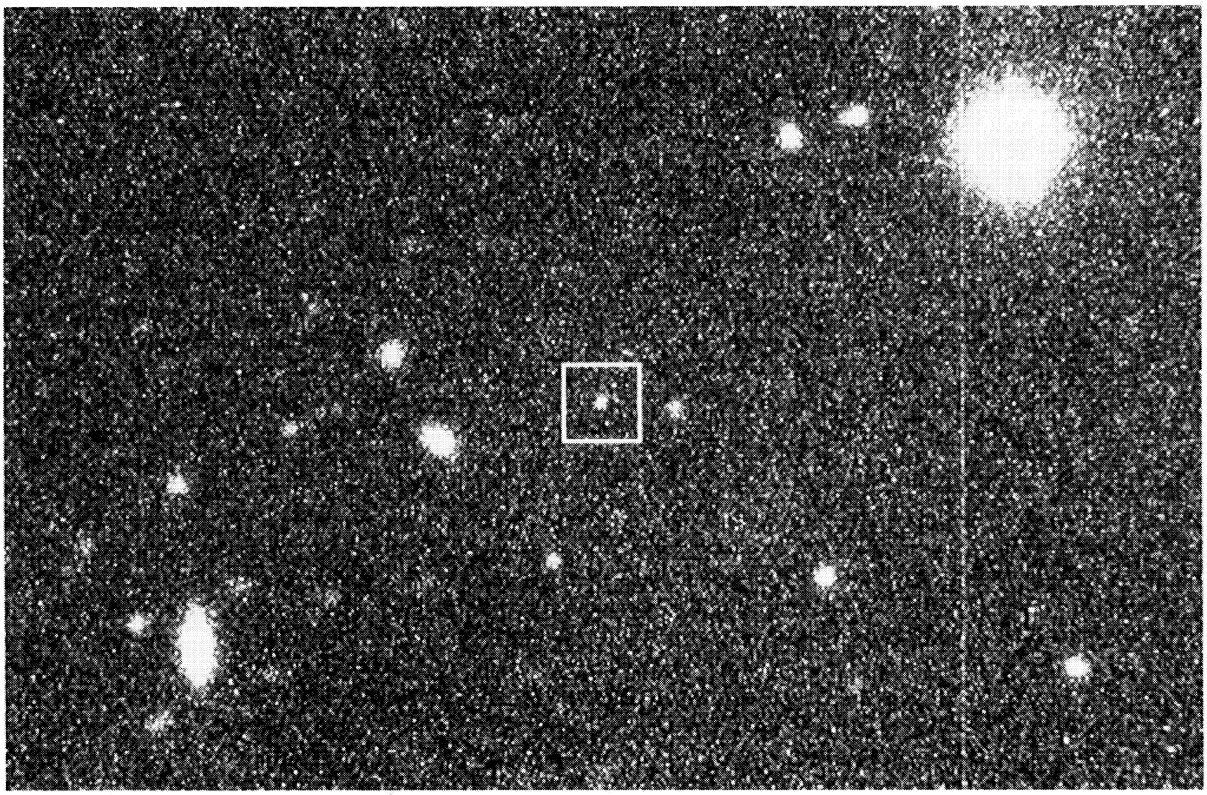

FIG. 1. Sample of part of a CCD image from the Mauna Kea survey. Parameters of the image are integration time 900 s through an *R* filter, north is to the top, east to the left, and the 10 arcsec wide box marks 1993 FW (magnitude 23.3). The image was taken UT 1993 March 28 at the University of Hawaii 2.2 m telescope.

D. C. Jewitt and J. X. Luu (see page 1868)